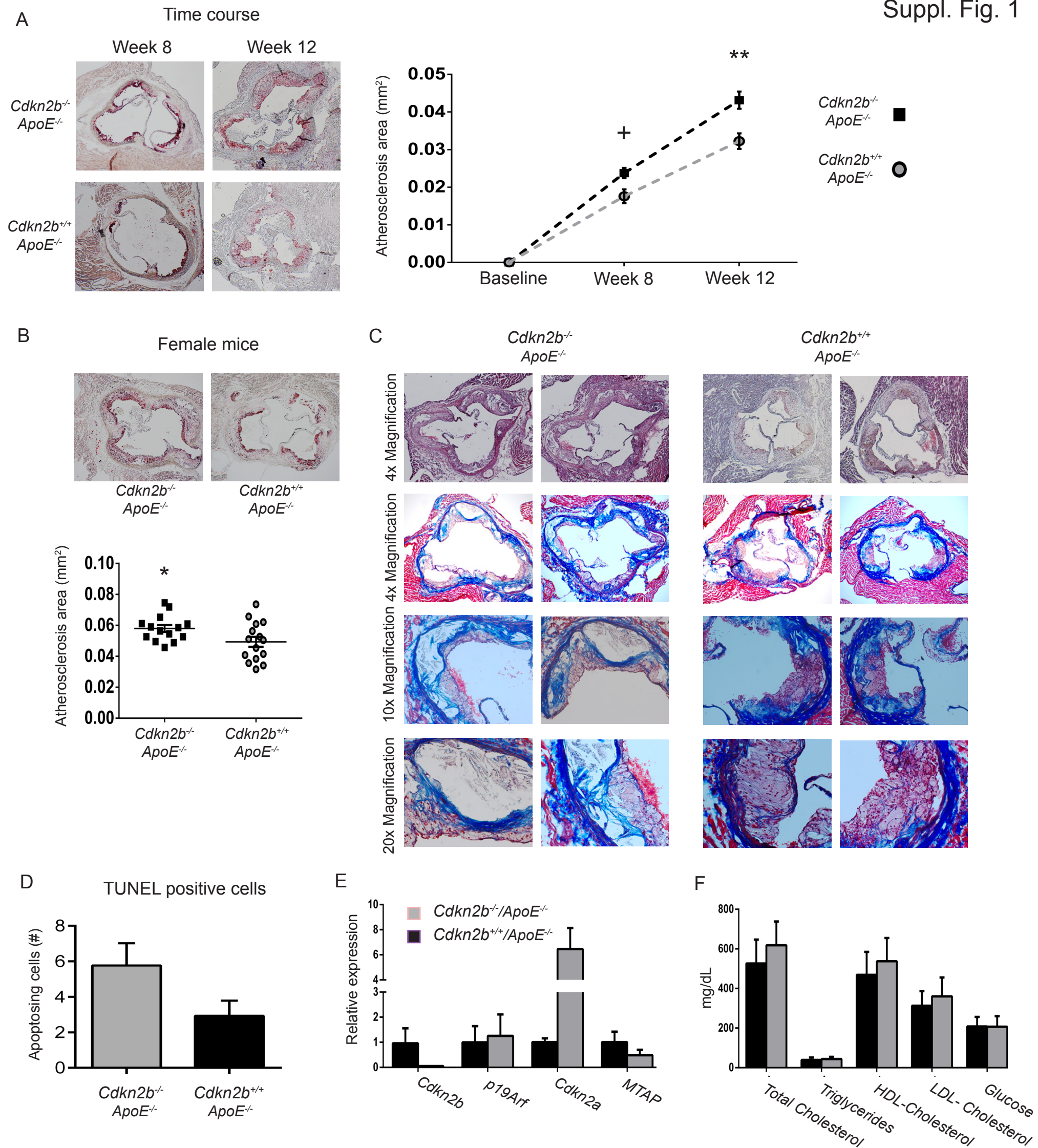
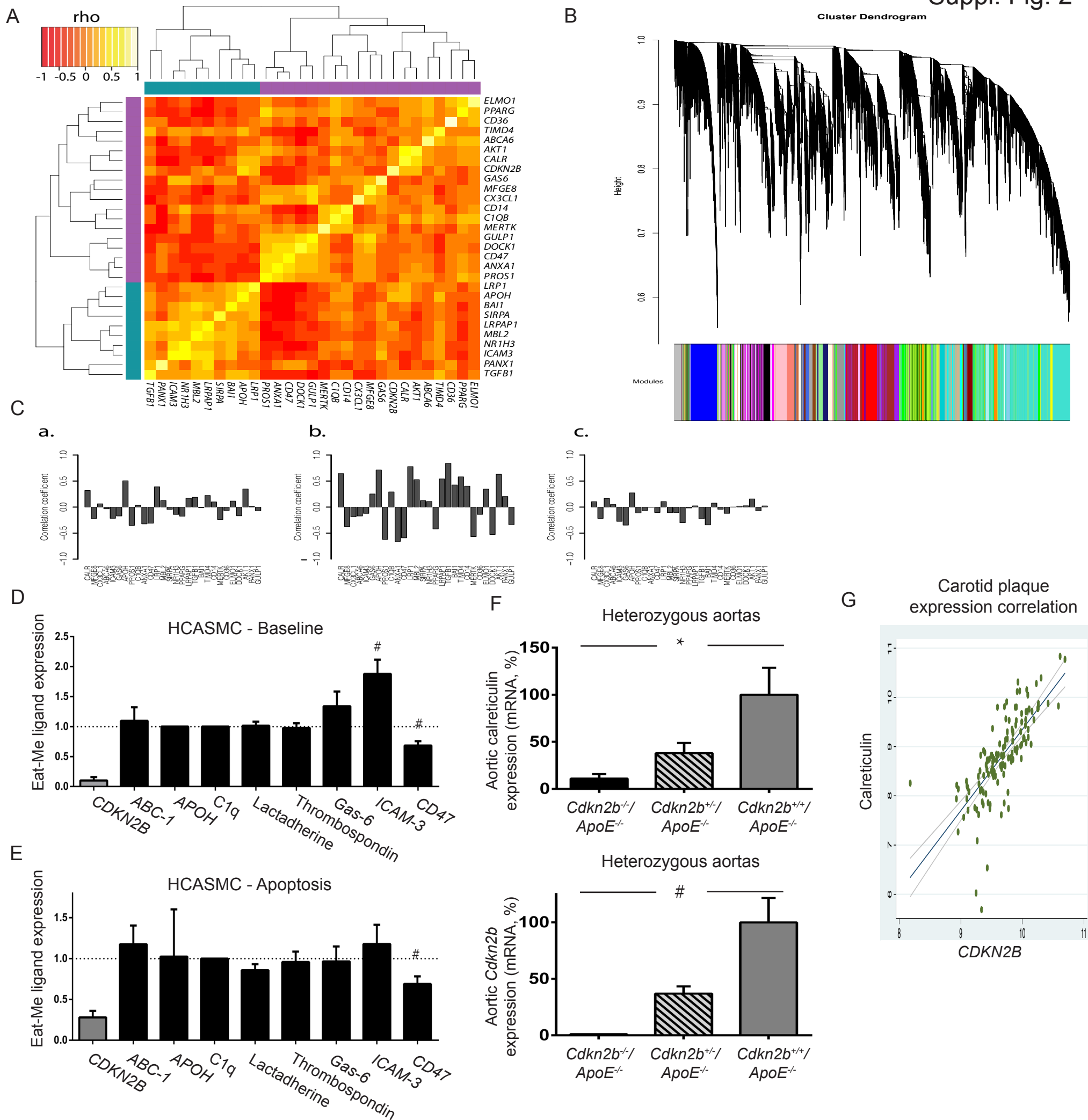


Supplemental Figure 1. Loss of *Cdkn2b* promotes atherosclerosis in both genders and at serial timepoints. Loss of *Cdkn2b* also increases growth of the necrotic core and increases early apoptosis. (A) Relative to male *Cdkn2b*^{+/+},*ApoE*^{-/-} control mice, male *Cdkn2b*^{-/-},*ApoE*^{-/-} mice develop advanced atherosclerotic plaques as soon as 8 weeks after initiating Western diet, with these changes persisting over time (4x magnification). (B) A similar change is observed in female mice ($P=0.04$, 4x magnification). (C) Additional examples of the large acellular necrotic cores observed in *Cdkn2b*^{-/-},*ApoE*^{-/-} mice relative to *Cdkn2b*^{+/+},*ApoE*^{-/-} control animals (H&E staining on top, Masson Trichrome on bottom at various magnifications). (D) Because very little apoptosis was observed at the terminal endpoint of the chronic model provided in Figure 1, an additional 10 *Cdkn2b*^{+/+},*ApoE*^{-/-} and *Cdkn2b*^{-/-},*ApoE*^{-/-} who had only received 4 weeks of high-fat diet were infused with Angiotensin II by osmotic minipump for 72 hours prior to sacrifice to induce acute vascular inflammation. In this case, *Cdkn2b*^{-/-},*ApoE*^{-/-} displayed a 97% increase in TUNEL positive cells per section relative to controls, of borderline significance ($P=0.06$). (E) Compensation of other 9p21.3 locus genes in aortic tissue from *Cdkn2b*^{-/-},*ApoE*^{-/-} relative to *Cdkn2b*^{+/+},*ApoE*^{-/-} control mice. As previously described, there is significant upregulation of *Cdkn2a* in *Cdkn2b* knockout animals. In the current studies, no difference in the expression of the pro-apoptotic gene *p19/Arf* was observed at the terminal endpoint. (F) No difference in lipid levels or fasting glucose was observed between genotypes after 12 weeks of Western diet.

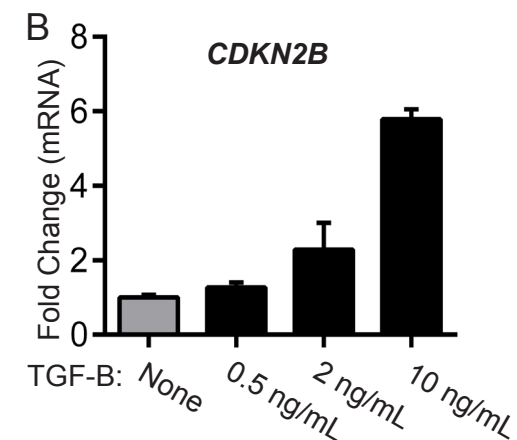
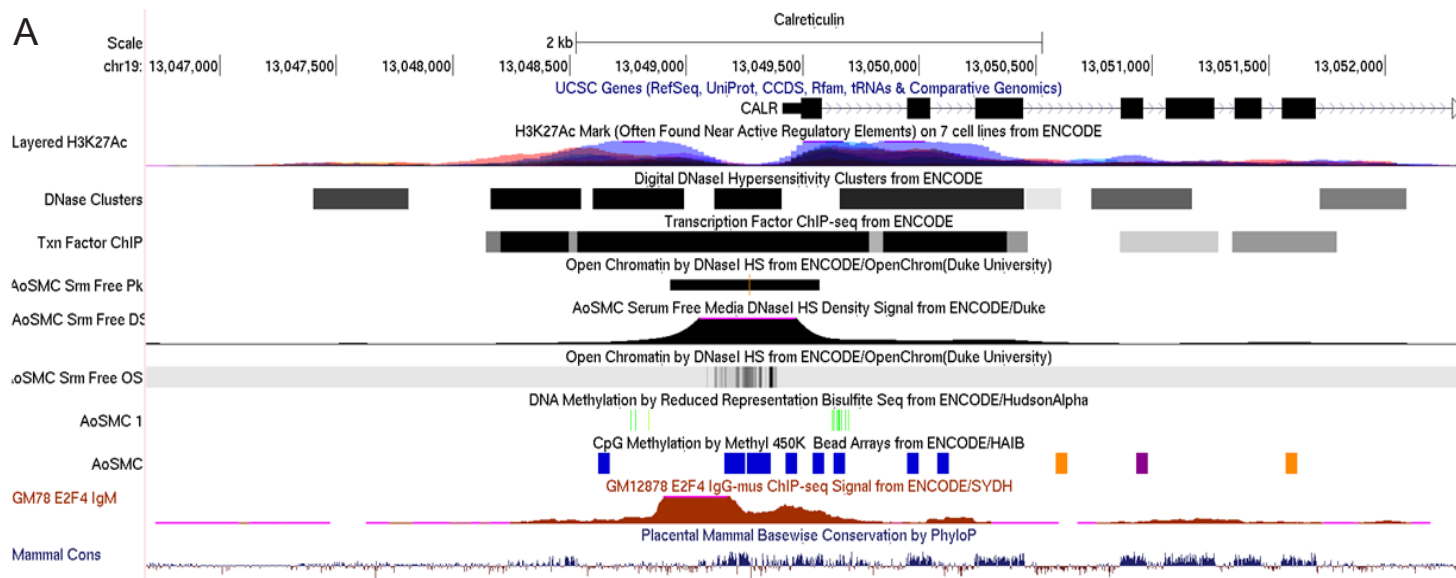


Supplemental Figure 2. Bioinformatics analysis of human atherosclerosis samples and evaluation of additional efferocytosis genes in HCASMC. (A) Topological relationship between *CDKN2B* and genes involved in efferocytosis in human coronary artery segments. Color bars correspond to module assignment. (B) Gene coexpression network cluster dendrogram from human coronary artery segments. The network adjacency was calculated from topological overlap between all gene pairs represented in the expression data set. The dynamic tree cut algorithm was used to iteratively choose stable cluster sizes and partition the network into modules. (C) Correlation between *CDKN2B* expression and genes involved in efferocytosis in human coronary artery segments: (a) All samples; (b) samples without atherosclerotic lesions; (c) samples with atherosclerotic lesions. (D) Relative expression of several additional candidate efferocytosis genes in si*CDKN2B* HCASMC compared to siCont HCASMC at baseline (D) and during apoptosis (E). (F) Compared to control *Cdkn2b*^{+/+},*ApoE*^{-/-} specimens, aortas from female heterozygous *Cdkn2b*^{+/-},*ApoE*^{-/-} had an intermediate 62.1% reduction in *Calr* expression ($P < 0.03$) compared to the 90.8% reduction in *Calr* expression observed in *Cdkn2b*^{-/-},*ApoE*^{-/-} animals ($P < 0.02$, top panel). These findings correlated with the in vivo reduction of aortic *Cdkn2b* expression observed in heterozygous animals (bottom panel). (G) Co-expression analysis in human carotid artery atherosclerotic plaques confirm that *CDKN2B* and *CALR* are positively associated, as observed in human coronary artery atherosclerotic plaque ($r^2 = 0.74$, $P < 0.0001$).



Supplemental Figure 3. Additional analysis of the *CALR* promoter. (A) Publically-available data from the UCSC genome browser reveals that the *CALR* promoter has an open chromatin pattern, DNase hypersensitivity sites, a consistent AoSMC DNA methylation pattern and published ChIP-seq data all of which suggest that E2F4 could regulate *CALR* expression in human SMCs. (B) Untransfected HCASMC increased their expression of *CDKN2B* in response to exogenous TGF- β stimulation in a pattern consistent with the luciferase reporter data shown in Figure 3. (C) *CALR* promoter oligo sequences and ChIP primers employed in the EMSA and immunoprecipitation studies, respectively, described in Figure 3. (D) Positive and negative control reactions employed in the EMSA experiments for Figure 3.

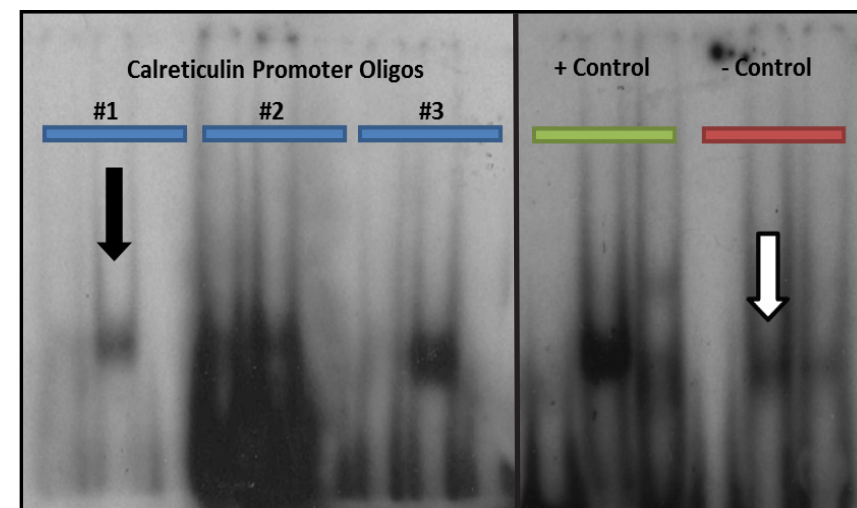
Suppl. Fig. 3



C

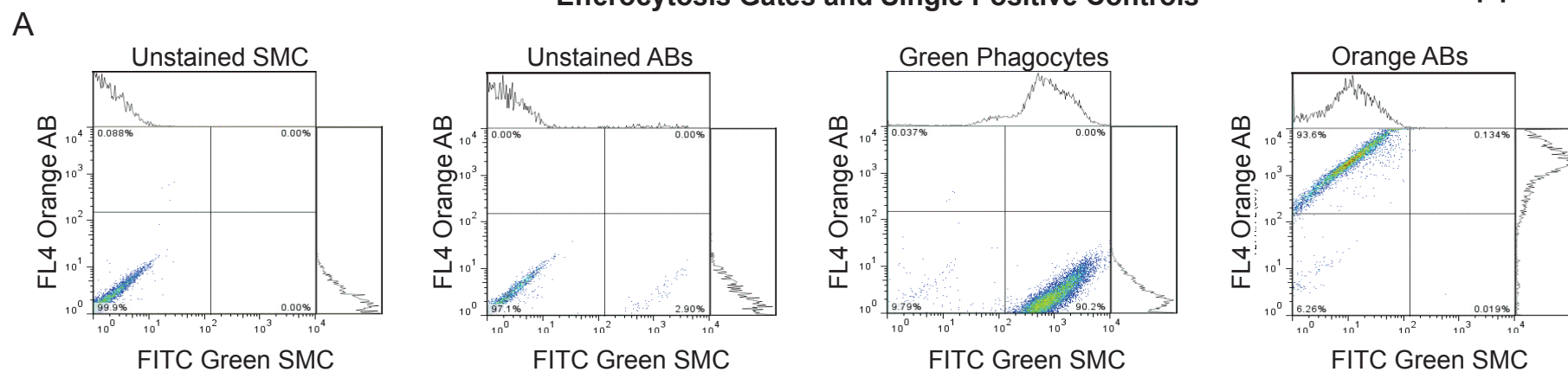
Condition	Name	Sequence
ChIP Primers		
CRT Promoter	E2F4 ChIP F	AGGTCCAATGGAAAAAGAC
	E2F4 ChIP R	CAGAAACTGCTCCTTGAAGT
Positive Control	FGF2 prom ChIP F	CTGTTTTCAGTGCCAACT
	FGF2 prom ChIP R	CATGGGGCCCCGTCGGCCGCTG
Negative Control	E2F4 Neg ChIP F	CCGGAAGCACTTCTCCTAGA
	E2F4 Neg ChIP R	AAGAGAGAGCGGAAGTGACG
Gel Shift Oligos		
CRT Promoter	CRT E2F4 F	TGGCAGGGGCGGGCCCAAGGGCTG
	CRT E2F4 R	CAGCCCTTGGGCCCCCCTGCCA
Mutagenesis	CRT E2F4 * F	CAATGACAAAGTGGCAGGTATTGCCCAAGGGCTGGGTCAGG
	CRT E2F4 * R	CCTGACCCAGCCCTTGGGCAATACCCTGCCACTTTGTCATTG
Positive Control	Consensus E2F F	ATTTAAGTTTCGCGCCCTTTCTCAA
	Consensus E2F R	TTGAGAAAGGGCGCGAAACTTAAAT

D

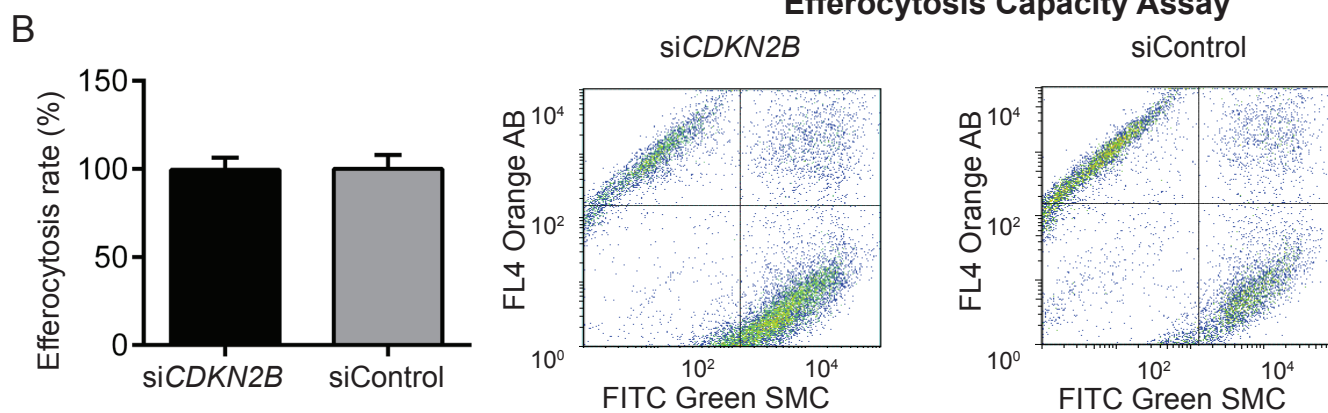


Supplemental Figure 4. *CDKN2B* does not alter the phagocytic capacity of the neighboring cell. (A) Control gates employed for all efferocytosis studies. (B) Although loss of *CDKN2B* rendered apoptotic cells resistant to efferocytosis, loss of *CDKN2B* in the neighboring, non-apoptotic HCASMC had no impact on its phagocytic capacity. Note that *CDKN2B* was undetectable in 'professional' phagocytes such as macrophages, in culture. (C) Apoptotic primary *Cdkn2b*^{-/-} aortic smooth muscle cells resist phagocytic clearance by RAW macrophages relative to apoptotic primary *Cdkn2b*^{+/+} aortic smooth muscle cells ($P < 0.01$), in keeping with findings provided for *CDKN2B*-deficient HCASMC in Figure 4. (D) Heterozygous *Cdkn2b*^{+/-} aortic smooth muscle cells show an intermediate efferocytosis phenotype. (E) Additional examples of failed efferocytosis in vivo in *Cdkn2b*^{-/-}, *ApoE*^{-/-} mice. Electron micrographs at various magnifications again reveal more frequent apoptosis and necrosis in *Cdkn2b*^{-/-}, *ApoE*^{-/-} animals, with condensed chromatin and interruption of plasma membrane integrity (black arrows), along with a high burden of extracellular debris and ABs not associated with an adjacent macrophage (black arrowheads). Conversely, *Cdkn2b*^{+/+}, *ApoE*^{-/-} control mice displayed smoothly outlined nuclei with normal heterochromatin patterns, normal sized mitochondria and intact plasma membranes (white arrowheads). These plaques also routinely displayed macrophages which had ingested numerous ABs, suggestive of intact efferocytosis.

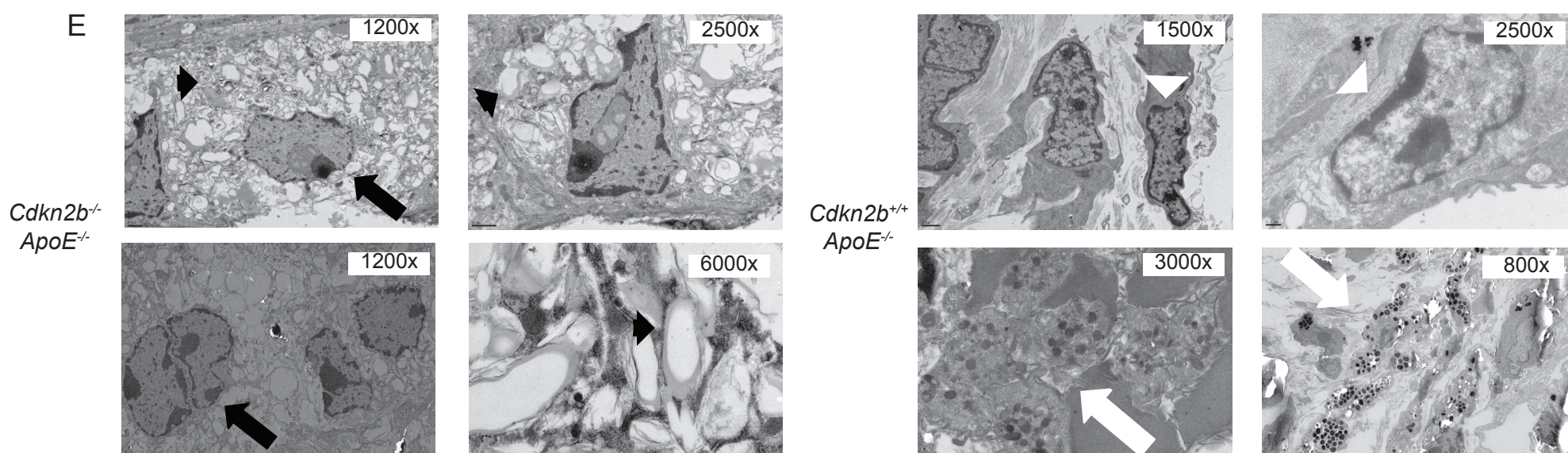
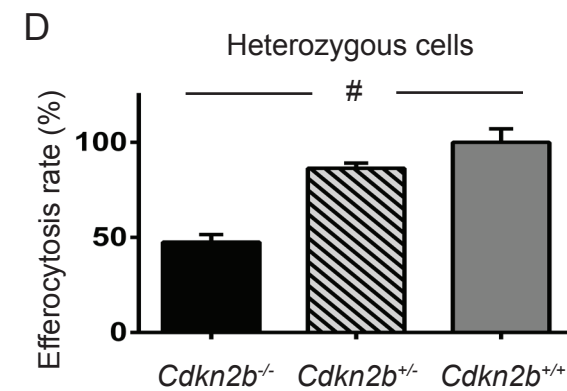
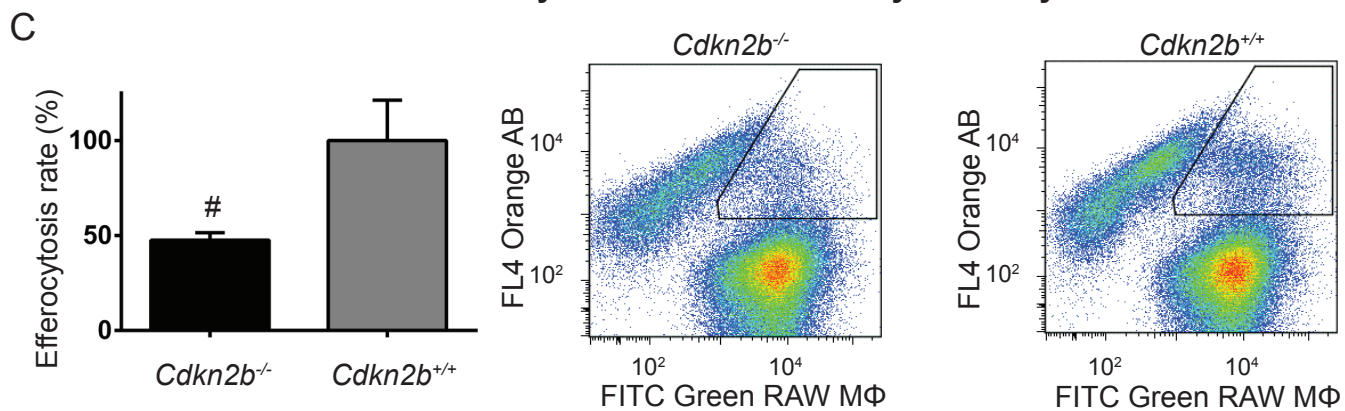
Efferocytosis Gates and Single Positive Controls



Efferocytosis Capacity Assay



Efferocytosis Resistance Assay - Primary Mouse Aortic Smooth Muscle Cells



Supplemental Figure 5. Macrophages co-cultured with *Cdkn2b*^{+/+} AB (grey bar) upregulated *Abca1* relative to baseline (white bar). This homeostatic pathway was significantly blunted when macrophages were co-cultured with *Cdkn2b*^{-/-} AB (black bar), as observed for the experiments with *CDKN2B*-deficient HCASMCs provided in Figure 5.

Supplemental Table 1. Summary of topological characteristics of gene coexpression modules identified in human coronary artery segments.

Supplemental Table 2. Summary of gene coexpression module assignment in human coronary artery segments. *k*Total = global network connectivity, *k*Within = intramodular network connectivity, *k*Out = extramodular network connectivity, *k*Diff = difference between extramodular and intramodular connectivity, MAR = maximum adjacency ratio, *k*MEO...*k*MEn = correlation between gene expression and module eigengene expression for modules 0...n.

Supplemental Table 3. Primers and probes used in these studies.

